

Directed flow of antiprotons in Au+Au collisions at AGS

J. Barrette^e, R. Bellwiedⁱ, S. Bennettⁱ, R. Bersch^g,
 P. Braun-Munzinger^b, W. C. Chang^g, W. E. Cleland^f,
 M. Clemen^f, J. Cole^d, T. M. Cormierⁱ, Y. Dai^e, G. David^a,
 J. Dee^g, O. Dietzsch^h, M. Drigert^d, S. Esumi^c, K. Filimonov^c,
 A. Frenchⁱ, S. C. Johnson^g, J. R. Hallⁱ, T. K. Hemmick^g,
 N. Herrmann^c, B. Hong^b, Y. Kwon^g, R. Lacasse^e, Q. Liⁱ,
 T. W. Ludlam^a, S. K. Mark^e, S. McCorkle^a, D. Miśkowiec^b,
 E. O'Brien^a, S. Panitkin^g, V. Pantuev^g, P. Paul^g, T. Piazza^g,
 M. Pollack^g, C. Pruneauⁱ, Y. J. Qi^e, E. Reber^d, M. Rosati^e,
 S. Sedykh^g, J. Sheenⁱ, U. Sonnadara^f, J. Stachel^c,
 N. Starinski^e, E. M. Takagui^h, V. Topor Pop^e, M. Trzaska^g,
 S. Voloshinⁱ, T. B. Vongpaseuth^g, G. Wang^e, J. P. Wessels^c,
 C. L. Woody^a, N. Xu^g, Y. Zhang^g and C. Zou^g
 (E877 Collaboration)

^aBrookhaven National Laboratory, Upton, New York 11973

^bGesellschaft für Schwerionenforschung, 64291 Darmstadt, Germany

^cPhysikalishes Institut, Universität Heidelberg, 69120 Heidelberg, Germany

^dIdaho National Engineering Laboratory, Idaho Falls, Idaho 83402

^eDepartment of Physics, McGill University, Montréal, Québec, Canada H3A 2T8

^fDepartment of Physics and Astronomy, University of Pittsburgh, Pittsburgh, Pennsylvania 15260

^gDepartment of Physics and Astronomy, State University of New York at Stony Brook, New York 11794

^hDepartment of Physics, University of São Paulo, 05508 São Paulo, Brazil

ⁱPhysics Department, Wayne State University, Detroit, Michigan 48202

Abstract

Directed flow of antiprotons is studied in Au+Au collisions at a beam momentum of 11.5A GeV/c. It is shown that antiproton directed flow is anti-correlated to proton flow. The measured transverse momentum dependence of the antiproton flow is compared with predictions of the RQMD event generator.

1 Introduction

The production of antiprotons at AGS energies (10-15A GeV) is near threshold in nucleon-nucleon collisions. Via collective effects, \bar{p} production can be enhanced in nucleus-nucleus collisions as compared to p+p collisions [1-4]. The observed yield of antiprotons is a result of both production and subsequent annihilation. The high antiquark densities in the quark-gluon plasma (QGP) state might lead to antibaryon abundances greatly exceeding the values in a chemically equilibrated hadron gas [5]. However, due to conservation of entropy, those abundances may be considerably diluted to a level very close to chemical equilibrium [6]. On the other hand, antibaryons have a large annihilation cross section, which may be modified in the baryon rich colliding systems [7]. Measurements of \bar{p} at the AGS may also contain a large feed-down contribution from the decay of antilambdas, $\bar{\Lambda} \rightarrow \bar{p} + \pi^+$, as well as from other antihyperons (\bar{Y}). Microscopic calculations have given some indication of how the annihilation process might change in the dense environment of a heavy-ion collision. It has been shown that the amount of annihilation in the nuclear medium depends strongly on the formation time of the hadrons [8]. In view of all this, it came as a surprise that both in Si+Au and Au+Au collisions the measured \bar{p}/p ratio is well described by computing the yields from a fireball in complete thermal and chemical equilibrium [9,10]. Since the conditions for thermal equilibrium are equal to those for hydrodynamic evolution of the fireball, it is of great interest to determine experimentally the flow features for antiprotons.

The hydrodynamic evolution of the fireball leads to characteristic flow patterns such as radial expansion [9] and azimuthal anisotropies, first discovered in ultra-relativistic nuclear collisions by ref. [11]. Since then, the study of anisotropies in the azimuthal distribution of particles, also called anisotropic (directed, elliptic, etc.) transverse flow, plays an important role in high energy nuclear collisions [12-14]. Detailed measurements (for surveys see refs. [15,16]) have revealed that in a non-central high energy heavy-ion collision, nucleons in the backward hemisphere are preferentially emitted in the direction of the impact parameter vector pointing from the target to the projectile. Antiprotons co-moving with those nucleons have a greater probability of annihilation and rescattering, and this could result in an anticorrelation with the nucleon directed flow - the so-called *anti-flow* of antiprotons in nuclear collisions predicted by Jahns *et al.* [17,18]. Measurements of the directed flow of antiprotons are important for understanding the role of annihilation in dense nuclear matter. They could also provide insight into the mechanism of anti-

quark production in heavy-ion collisions. A surprising result reported in refs. [19,20], is the possible anomalous enhancement of the $\bar{\Lambda}/\bar{p}$ ratio even beyond values expected for complete chemical equilibration [9]. One possible explanation could be that $\bar{\Lambda}$ baryons have a lower annihilation cross section than \bar{p} . A straightforward way to test this hypothesis would be the measurement of \bar{p} and $\bar{\Lambda}$ (*anti-*)flow [21].

Antiproton production in heavy-ion induced reactions at the AGS has been studied experimentally by the E858/E878 [22,23], E814/E877 [24,25], E866 [26], E886 [27], E864 [28,19], E802 [29,30], and E917 [20] collaborations. In the current paper we present the first results on the measurements of directed flow of antiprotons detected in the E877 spectrometer in Au+Au collisions at a beam momentum of 11.5A GeV/c. The results were obtained from the analysis of 46 millions of central Au+Au events recorded during the 1995 heavy-ion run.

2 E877 apparatus

Fig. 1 shows the E877 experimental setup which is also discussed in [11,31,32]. The trajectory of each beam particle was measured by two silicon micro-strip beam vertex detectors (BVER), located at 2.8 m and 5.8 m upstream of the target. For the 1995 run, each detector was upgraded from single-sided silicon wafers with one-dimensional pitch of 50 μm to double-sided wafers with a 200 μm pitch in both the x and y directions [33]. Using these detectors the coordinates and angle of beam particles at the target were determined with an accuracy of 300 μm in position and 60 μrad in angle.

The determination of the centrality of the collision and of the reaction plane orientation were done using the transverse energy distribution measured in the target calorimeter (TCAL), and participant calorimeter (PCAL). Both calorimeters had 2π azimuthal coverage and, combined, provided nearly complete polar angle coverage: TCAL and PCAL covered the pseudorapidity regions $-0.5 < \eta < 0.8$ and $0.8 < \eta < 4.2$, respectively [31].

Charged particles emitted in the forward direction and passing through a collimator ($-134 \text{ mrad} < \theta_{\text{horizontal}} < 16 \text{ mrad}$, $-11 \text{ mrad} < \theta_{\text{vertical}} < 11 \text{ mrad}$) were analyzed by a high resolution magnetic spectrometer with a horizontal bend-plane. The spectrometer acceptance covered mostly the forward rapidity region. The momentum of each particle was measured using two drift chambers, DC2 and DC3, whose pattern recognition capability was aided by four multi-wire proportional chambers (MWPC). The average momentum resolution was $\Delta p/p \approx 3\%$, limited by multiple scattering. A time-of-flight hodoscope (TOFU) located directly behind the tracking chambers provided the

time-of-flight information with an average resolution of 85 ps. Energy loss measurements in TOFU and in a Forward Scintillator (FSCI) array located approximately 30 m downstream of the target were used to determine the particle charge.

For the 1995 run, the spectrometer was upgraded with upstream tracking chambers. Two identical multi-wire proportional chambers with highly segmented chevron-shaped readout pads, VTXA and VTXB, were instrumented and placed at 2 m and 2.25 m downstream of the target, just in front of the spectrometer magnet. They provided a precise measurement (about $300 \mu\text{m}$ resolution) of the track coordinate in the bending plane of the spectrometer before deflection in the magnetic field. A description of the design, implementation and performance of the vertex detectors can be found in [34].

3 Antiproton identification

The particle identification was performed by combining measurements of momentum, velocity, and charge of the particle. To reduce the background in the identification of antiprotons, tracks were required to have a confirmation from both upstream VTX detectors. Tracks were also required to have complete information from the cathode pad readout in both drift chambers. Fig. 2 shows the distribution of particle mass squared, calculated from the measured momentum and velocity, for negative particles with momentum less than 4 GeV/c. A clear antiproton peak is seen, with good signal-to-background ratio. The contribution of the background increases with momentum (see lower panel of Fig. 2) and becomes dominant at $p > 4.5 \text{ GeV}/c$. A maximum momentum of 4 GeV/c was required for clean identification of antiprotons. The mass resolution is quantitatively understood in terms of the intrinsic detector resolution, multiple scattering and time-of-flight resolution. For a positive antiproton identification we selected, in a plot of momentum versus the measured mass, a region of $\pm 2.0\sigma_{m^2}(p)$ around the antiproton mass peak, where $\sigma_{m^2}(p)$ represents the resolution in the mass squared at a given particle momentum p . The dependence of the mass resolution on momentum was assumed to be equal to that of protons.

Fig. 3 shows the antiproton acceptance in the transverse momentum p_t and rapidity y coordinates. The E877 spectrometer mainly covers the low p_t region ($p_t < 0.4 \text{ GeV}/c$) forward of $y_{cm} = 1.6$ ($1.6 < y < 2.2$). The final data sample comprises about 750 antiprotons with about 400 in the $1.8 < y < 2.2$ rapidity region.

Since tracking only starts 2 m downstream of the target, the E877 spectrometer is not well suited for separation of primary antiprotons from those fed

down from anti-hyperon decays. Because of the large mass asymmetry and small decay momentum in these decays, the antiproton track points back to the target. A previous extensive study [35] based on a Monte-Carlo simulation showed that antiprotons are reconstructed for 70% of the $\bar{\Lambda}$ and for 100% of the Σ^- decaying such that the \bar{p} is emitted into the acceptance of the spectrometer and consistent with originating from the target.

4 Results and Discussion

4.1 Experimental data

The azimuthal anisotropy in particle production is studied by means of Fourier analysis of azimuthal distributions [11,31,32,36,37] with respect to the reaction plane. We study the rapidity, transverse momentum, and centrality dependence of the Fourier coefficients v'_n (amplitude of n -th harmonic) in the decomposition:

$$E \frac{d^3N}{d^3p} = \frac{1}{2\pi} \frac{d^2N}{p_t dp_t dy} (1 + 2v'_1 \cos \phi + 2v'_2 \cos 2\phi + \dots),$$

where the azimuthal angle $\phi = \phi_{lab} - \psi_r$ is taken with respect to the reaction plane orientation. Directed flow is quantified by the dipole Fourier coefficient v'_1 .

Similarly to the analysis performed in [31,32], the reaction plane angle is determined from the measured transverse energy distribution in four non-overlapping pseudorapidity windows. The *reaction plane resolution*, i.e. the accuracy with which the reaction plane orientation is determined, is evaluated by studying the correlation between flow angles measured in different windows. Finally, the flow signals are corrected for the finite reaction plane resolution. Details of this procedure are described in [31,32]. In the following, only coefficients v_1 corrected for the reaction plane resolution will be shown.

The experimental acceptance for \bar{p} is close to mid-rapidity (Fig. 3), where the directed flow changes sign. To optimize a possible flow signal, we skip the region very close to mid-rapidity and present, in Fig. 4, the measured azimuthal distributions of antiprotons emitted at rapidity $y > 1.8$, for two collision centralities. To determine v_1 , the distributions were fitted with a distribution $f(\phi) = 1 + 2v_1 \cos \phi$. A pronounced minimum is observed at $\phi = 0$ for semicentral collisions ($\sigma = 10 - 26\% \sigma_{geo}$), indicating that the antiproton production is strongly anti-correlated with the flow of nucleons. For more central collisions (top 10% of σ_{geo}), the antiproton azimuthal distribution is, within

errors, isotropic ($v_1 \approx 0$). No or very little proton flow has been observed for the most central Au+Au collisions [32].

The measured transverse momentum dependence of v_1 is shown in Fig. 5. Large negative values of v_1 are observed for $p_t > 0.1$ GeV/c. It should be noted that the absolute value of the proton flow signal at similar rapidities and transverse momenta is significantly smaller [32]. The right hand panel shows a result consistent with zero flow for the more central bin.

4.2 RQMD predictions

The Relativistic Quantum Molecular Dynamics (RQMD) model [38] has been widely used in describing relativistic heavy-ion collisions. It combines classical propagation of all hadrons with string and resonance excitations in the primary collisions of nucleons from target and projectile. Overlapping color strings may fuse into so-called ropes [39]. Subsequently, the fragmentation products from rope, string and resonance decays interact with each other and with the original nucleons, mostly via binary collisions. These interactions drive the system towards equilibration [40] and are responsible for the development of collective flow, even in the pre-equilibrium stage. If baryons are surrounded by other baryons they acquire effective masses. These effective masses are generated by introducing Lorentz-invariant Skyrme-type quasi-potentials into the mass-shell constraints for the momenta, which simulates the effect of a *mean field* [41]. There are no potential-type interactions in the so-called *cascade mode* of RQMD.

For antiprotons, RQMD combines a large enhancement of initial production via hadronic multi-step processes with strong absorption through the free \bar{p} absorption cross section [42], which results in the absorption of a large fraction of the produced antiprotons ($\approx 90\%$ of \bar{p} are reabsorbed for minimum bias Au+Au collisions [18]). The newest version of the model (RQMD v2.3) uses the formation of a quasi-bound state (proton-antiproton molecule) to significantly reduce the possibility of antiproton annihilation. However, the presence of a mean color potential could possibly have a much more significant effect on the final antiproton distribution [43]. A systematic study of the antibaryon production with various projectile-target combinations and at different energies would be useful for refining this approach and for understanding the annihilation process in relativistic heavy-ion collisions.

Predictions of the RQMD model run in *cascade mode* for the p_t -dependence of v_1 for antiprotons are compared to the data in Fig. 5. For the model, we only used antiprotons produced in the experimental acceptance window. The magnitude of the negative signal observed in the data for semicentral collisions is

comparable, within the errors, to that predicted by the model although, systematically, the model values are somewhat smaller. The p_t -integrated signal observed in the data is $v_1 = -0.10 \pm 0.05$, compared to the predicted value of $v_1 = -0.06 \pm 0.06$.

A current question of interest and debate is the relative importance of including nuclear mean field effects in intra-nuclear cascade models at these energies. It is expected that collective flow may be an important observable for evaluating the importance of mean field effects [43]. It was shown, in particular that, in semicentral Au+Au collisions, protons exhibit a strong azimuthal anisotropy, with the amplitude of flow well reproduced by RQMD only if the effects of *mean field* are included [32]. It should be noted, however that, even including the mean field, only the p_t -integrated signal is reproduced by the model, while the predicted p_t -dependence significantly differs from the data. In Fig. 6 we present the RQMD v2.3 calculations for proton and antiproton mean values of the transverse momentum projected onto the reaction plane, $\langle p_x \rangle$, as a function of rapidity for Au+Au collisions at 11.5A GeV/c with impact parameters $b < 10$ fm. Calculations are presented for a pure cascade and mean-field modes of RQMD. Since the calculations are very CPU intensive we have a limited antiproton statistics for the mean field calculations: about 500 \bar{p} 's compared to more than 8700 \bar{p} 's for the cascade mode. The flow of nucleons is enhanced due to additional repulsion in the mean field approach. For antiprotons, on the other hand, the effective mean field potential in nuclear matter is expected to be attractive. The antinucleons are pulled towards the nucleon source, therefore the *anti-flow* should be considerably weakened [44], as observed in Fig. 6. Such a weakening is also supported by the results of Spieles *et al.* [43], where it was shown that, when the influence of the real part of an antinucleon-nucleus optical potential on the \bar{p} momentum spectra is included into the calculations, the antiproton annihilation is indeed suppressed in the heavy-ion environment, such that the sum of in-medium annihilation cross section and elastic cross section is closer to the free annihilation cross sections which are employed in the cascade mode of RQMD v2.3. On the other hand, the amplitude of the measured antiproton flow signal is rather well described by the pure cascade calculations (see Fig. 5). A similar observation has been recently made by comparing the measurements of K^+ directed flow with the cascade and mean field RQMD predictions [45], where it has been shown that the cascade calculations reproduce the data better than the mean field calculations. Further measurements and detailed calculations in the *mean field mode* are required and this question cannot be fully settled until antiproton yield and flow have been measured over a larger phase space.

5 Conclusion

We have observed, for the first time, a strong azimuthal anisotropy in antiproton production in semicentral Au+Au collisions which is anti-correlated with the nucleon emission. The observed large *anti-flow* for \bar{p} indicates that a strong annihilation process is involved in the dense nuclear matter as predicted by previous theoretical studies. The presented data have confirmed the need for a thorough investigation, both experimentally and theoretically, of antibaryon production in nucleus-nucleus interactions. Whereas the measured antiproton yields/spectra can be described within a thermal model assuming a chemical/thermal equilibration and collective expansion of the system, antiprotons exhibit a directed flow which is even stronger than expected by the models incorporating mean-field effects. A complementary measurement of the directed flow of antihyperons such as $\bar{\Lambda}$ in the future combined with our results would provide necessary information for the decoupling of the flow contribution of primary antiprotons and that of antihyperons. Furthermore, the comparison between the directed flow behavior of these two contributions could give crucial information for understanding the observed unexpected $\bar{\Lambda}/\bar{p}$ ratios.

Acknowledgments

We thank the AGS staff, W. McGahern and Dr. H. Brown for excellent support and acknowledge the help of R. Hutter in all technical matters. Financial support from the US DoE, the NSF, the Canadian NSERC, and CNPq Brazil is gratefully acknowledged.

References

- [1] S. Gavin, M. Gyulassy, M. Plümer and R. Venugopalan, Phys. Lett. B 234 (1990) 175.
- [2] V. Koch and C. B. Dover, Phys. Rev. C 40 (1989) 145.
- [3] V. Koch, G. E. Brown and C. M. Ko, Phys. Lett. B 265 (1991) 29.
- [4] J. Schaffner, I. N. Mishustin, L. M. Satarov, H. Stöcker and W. Greiner, Z. Phys. A 341 (1991) 47.
- [5] U. Heinz, P. R. Subramanian, H. Stöcker and W. Greiner, J. Phys. G: Nucl. Part. Phys. 12 (1986) 1237.
- [6] U. Heinz and H. Kowalski, Phys. Lett. B 233 (1989) 223.

- [7] S. H. Kahana, Y. Pang, T. Schlagel and C. B. Dover, Phys. Rev. C 47 (1993) 1356.
- [8] B. S. Kumar, S. V. Greene and J. T. Mitchell, Phys. Rev. C 50 (1994) 2152.
- [9] P. Braun-Munzinger, J. Stachel, J. P. Wessels and N. Xu, Phys. Lett. B 344 (1995) 43.
- [10] J. Stachel, Nucl. Phys. A 610 (1996) 509c; P. Braun-Munzinger and J. Stachel, Nucl. Phys. A 638 (1998) 3c.
- [11] J. Barrette et al., E877 Collaboration, Phys. Rev. Lett. 73 (1994) 2532.
- [12] See various contributions in Proceedings of the 13th International Conference on Ultra-Relativistic Nucleus-Nucleus Collisions, Quark Matter '97, Nucl. Phys. A 638 (1998).
- [13] H. Sorge, Phys. Rev. Lett. 82 (1999) 2048.
- [14] W. Cassing and E. L. Bratkovskaya, Phys. Reports 308 (1999) 65.
- [15] W. Reisdorf and H.G. Ritter, Annu. Rev. Nucl. Part. Sci. 47 (1998) 663.
- [16] N. Herrmann, J.P. Wessels and T. Wienold, Annu. Rev. Nucl. Part. Sci. 49 (1999) 581.
- [17] A. Jahns, C. Spieles, H. Sorge, H. Stöcker and W. Greiner, Phys. Rev. Lett. 72 (1994) 3464.
- [18] A. Jahns, C. Spieles, R. Mattiello, N.S. Amelin, H. Stöcker, W. Greiner and H. Sorge, Nucl. Phys. A 566 (1994) 483c.
- [19] T. A. Armstrong et al., E864 Collaboration, Phys. Rev. C 59 (1999) 2699.
- [20] B. B. Back et al., E917 Collaboration, Nucl. Phys. A 661 (1999) 75c.
- [21] S. A. Bass, M. Gyulassy, H. Stöcker and W. Greiner, J. Phys. G.: Nucl. Part. Phys. 25 (1999) R1.
- [22] M. Aoki et al., E858 Collaboration, Phys. Rev. Lett. 69 (1992) 2345.
- [23] M. J. Bennett et al., E878 Collaboration, Phys. Rev. C 56 (1997) 1521.
- [24] J. Barrette et al., E814 Collaboration, Phys. Rev. Lett. 70 (1993) 1763.
- [25] S. V. Green, Ph. D. Thesis, Yale University, 1992.
- [26] H. Sako for the E866 Collaboration, in *Heavy Ion Physics at the AGS (HIPAGS '96)*, C. A. Pruneau, G. Welke, R. Bellweid, S. J. Bennett, J. R. Hall and W. K. Wilson Eds., WSU-NP-96-16, Wayne State University, December 1996.
- [27] G. E. Diebold et al., E886 Collaboration, Phys. Rev. C 48 (1993) 2984.
- [28] F. Rotondo et al., E864 Collaboration, Nucl. Phys. A 610 (1996) 297c.
- [29] T. Abbott et al., E802 Collaboration, Phys. Rev. C 47 (1993) 1351.

- [30] L. Ahle et al., E802 Collaboration, Phys. Rev. Lett. 81 (1998) 2650.
- [31] J. Barrette et al., E877 Collaboration, Phys. Rev. C 55 (1997) 1420.
- [32] J. Barrette et al., E877 Collaboration, Phys. Rev. C 56 (1997) 3254.
- [33] Yi Dai, Ph. D. Thesis, McGill University, 1999.
- [34] R. Bersch, M. Sc. Thesis, SUNY at Stony Brook, 1995.
- [35] Y. Kwon, Ph. D. Thesis, SUNY at Stony Brook, 1997.
- [36] S. Voloshin and Y. Zhang, Z. Phys. C 70 (1996) 665.
- [37] J.-Y. Ollitrault, preprint nucl-ex/9711003.
- [38] H. Sorge, H. Stöcker and W. Greiner, Nucl. Phys. A 498 (1989) 567c.
- [39] H. Sorge, Phys. Rev. C 52 (1995) 3291.
- [40] H. Sorge, Phys. Lett. B 373 (1996) 16.
- [41] H. Sorge, Phys. Rev. Lett. 78 (1997) 2309.
- [42] A. Jahns, H. Stöcker and W. Greiner, Phys. Rev. Lett. 68 (1992) 2895.
- [43] C. Spieles, M. Bleicher, A. Jahns, R. Mattiello, H. Sorge, H. Stöcker and W. Greiner, Phys. Rev. C 53 (1996) 2011.
- [44] H. Sorge, private communication.
- [45] J. Barrette et al., E877 Collaboration, Nucl. Phys. A 661 (1999) 329c.

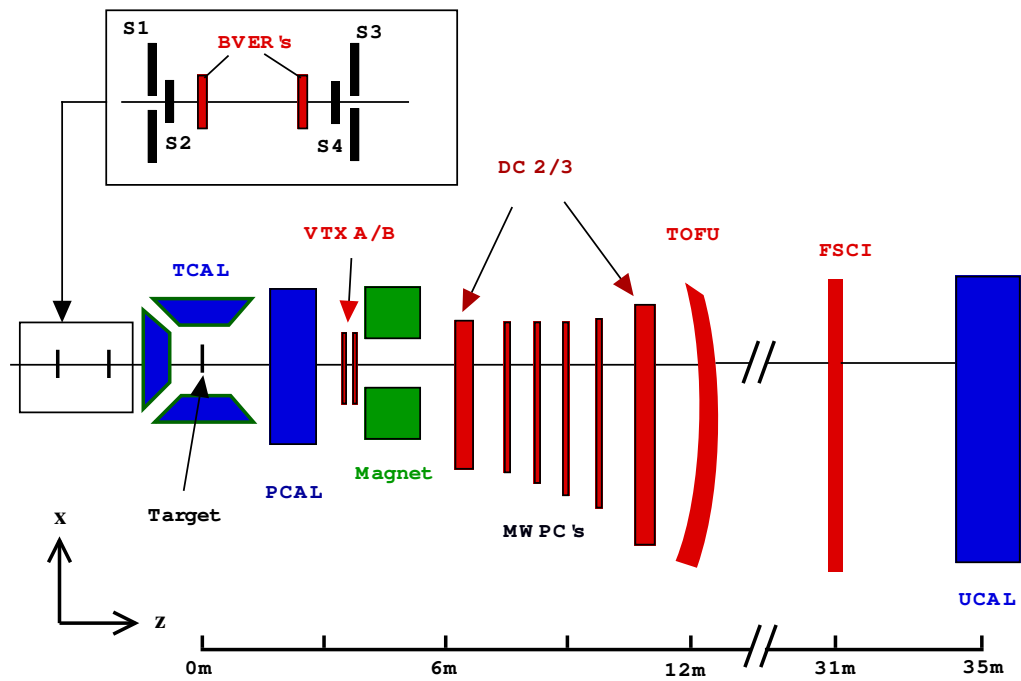


Fig. 1. E877 experimental setup.

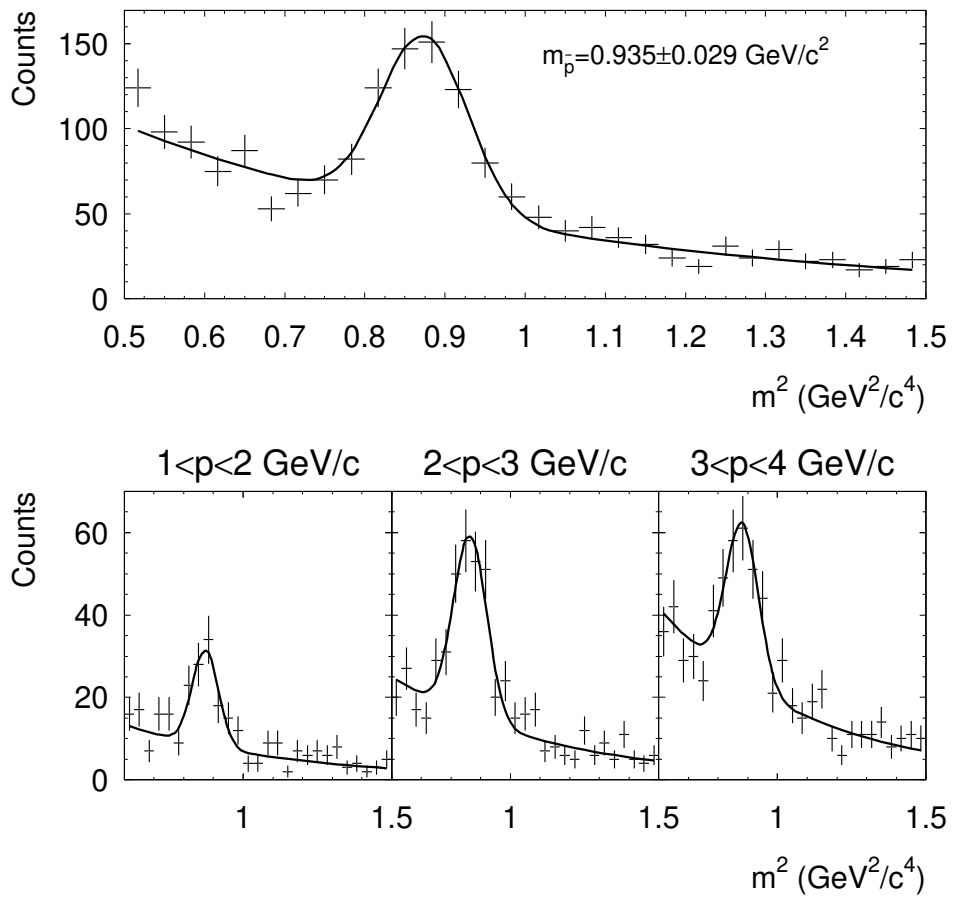


Fig. 2. Upper plot: the mass squared distribution in the antiproton peak region for negative particles with momenta less than 4 GeV/c. The Lower plot shows the same distribution for three different momentum intervals. The solid line is a fit by a Gaussian and an exponential.

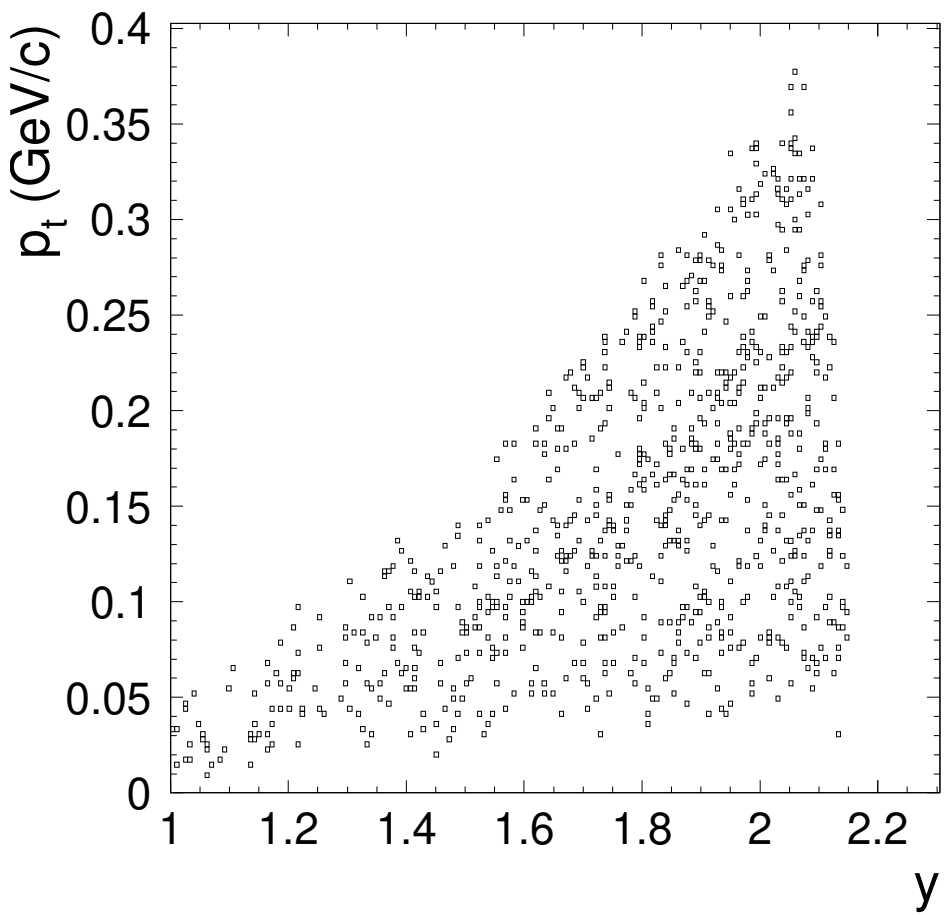


Fig. 3. Antiproton acceptance in the (p_t, y) phase space covered by the E877 spectrometer. Midrapidity is $y = 1.6$.

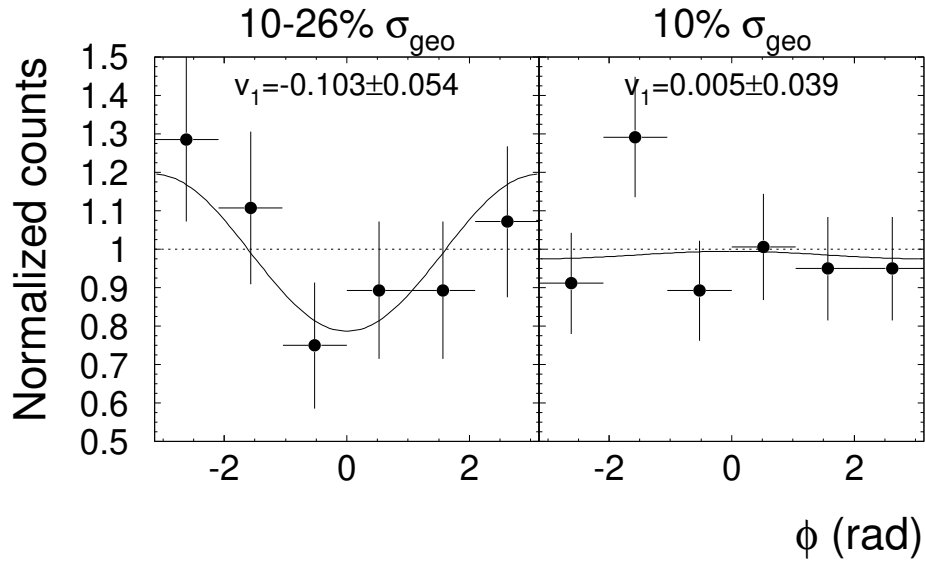


Fig. 4. Antiproton azimuthal distributions measured for rapidity $1.8 < y < 2.2$ and two collision centralities. The distributions are normalized such that the average is unity. The solid line is a fit by a $1 + 2v_1 \cos \phi$ distribution.

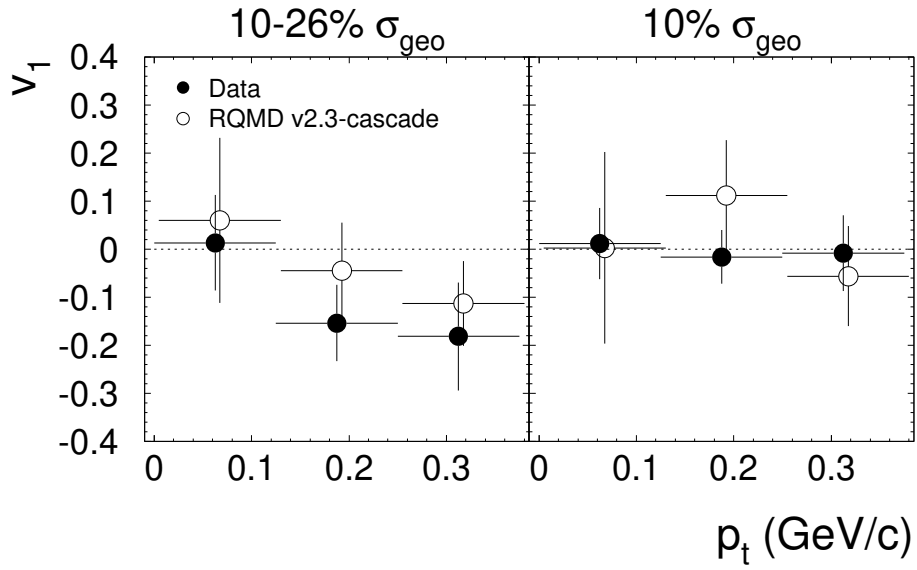


Fig. 5. $v_1(p_t)$ of antiprotons for rapidities $1.8 < y < 2.2$ and two collision centralities. The data (solid circles) are compared with the calculations using the RQMD v2.3 - *cascade mode* (open circles).

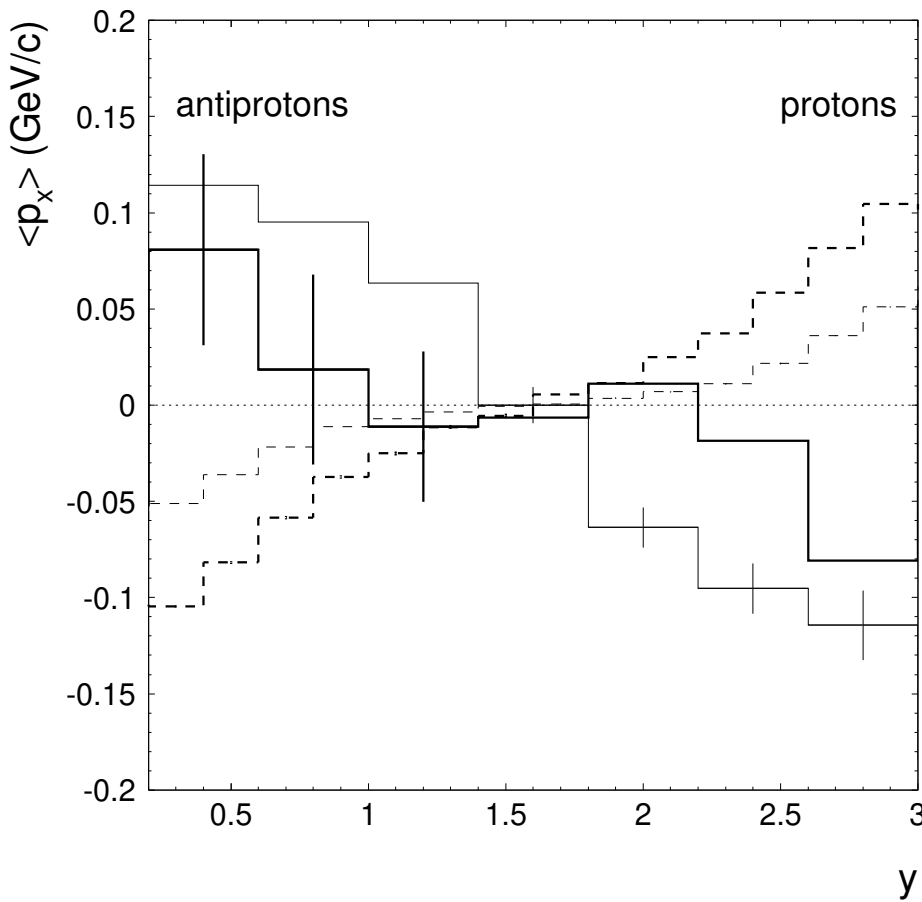


Fig. 6. Mean values of the transverse momentum projected into the reaction plane $\langle p_x \rangle$ of protons (dashed lines) and antiprotons (solid lines) as a function of rapidity for Au+Au collisions at 11.5A GeV/c with impact parameters $b < 10$ fm generated by using the RQMD v2.3 (*cascade mode* - thin lines; *mean field mode* - thick lines).